

This article was downloaded by: [Kobus, Jean-Michel]

On: 13 October 2010

Access details: Access Details: [subscription number 927964192]

Publisher Routledge

Informa Ltd Registered in England and Wales Registered Number: 1072954 Registered office: Mortimer House, 37-41 Mortimer Street, London W1T 3JH, UK



Journal of Sports Sciences

Publication details, including instructions for authors and subscription information:

<http://www.informaworld.com/smpp/title~content=t713721847>

Influence of free surface, unsteadiness and viscous effects on oar blade hydrodynamic loads

Alban Leroyer^a; Sophie Barré^{bc}; Jean-Michel Kobus^b; Michel Visonneau^a

^a Laboratoire de Mécanique des Fluides (UMR CNRS 6598), Equipe Modélisation Numérique, Ecole Centrale de Nantes, Nantes ^b Laboratoire de Mécanique des Fluides (UMR CNRS 6598), Equipe

Hydrodynamique Navale et Génie Océanique, Ecole Centrale de Nantes, Nantes ^c Ecole Nationale de Voile et des Sports Nautiques, Quiberon, France

First published on: 12 October 2010

To cite this Article Leroyer, Alban , Barré, Sophie , Kobus, Jean-Michel and Visonneau, Michel(2010) 'Influence of free surface, unsteadiness and viscous effects on oar blade hydrodynamic loads', Journal of Sports Sciences, 28: 12, 1287 – 1298, First published on: 12 October 2010 (iFirst)

To link to this Article: DOI: 10.1080/02640414.2010.485646

URL: <http://dx.doi.org/10.1080/02640414.2010.485646>

PLEASE SCROLL DOWN FOR ARTICLE

Full terms and conditions of use: <http://www.informaworld.com/terms-and-conditions-of-access.pdf>

This article may be used for research, teaching and private study purposes. Any substantial or systematic reproduction, re-distribution, re-selling, loan or sub-licensing, systematic supply or distribution in any form to anyone is expressly forbidden.

The publisher does not give any warranty express or implied or make any representation that the contents will be complete or accurate or up to date. The accuracy of any instructions, formulae and drug doses should be independently verified with primary sources. The publisher shall not be liable for any loss, actions, claims, proceedings, demand or costs or damages whatsoever or howsoever caused arising directly or indirectly in connection with or arising out of the use of this material.

Influence of free surface, unsteadiness and viscous effects on oar blade hydrodynamic loads

ALBAN LEROYER¹, SOPHIE BARRÉ^{2,3}, JEAN-MICHEL KOBUS², & MICHEL VISONNEAU¹

¹Laboratoire de Mécanique des Fluides (UMR CNRS 6598), Equipe Modélisation Numérique, Ecole Centrale de Nantes, Nantes, ²Laboratoire de Mécanique des Fluides (UMR CNRS 6598), Equipe Hydrodynamique Navale et Génie Océanique, Ecole Centrale de Nantes, Nantes, and ³Ecole Nationale de Voile et des Sports Nautiques, Quiberon, France

(Accepted 12 April 2010)

Abstract

Flow around a rowing blade is a very complex phenomenon, involving unsteady three-dimensional flow with violent motion of the free surface. However, in the literature, forces acting on blades are modelled using extreme and dubious simplifications. The aim of the present study was to evaluate the influence of free surface and unsteadiness (two physical characteristics that are commonly neglected when modelling loads on blades) as well as viscous effects. In fact, quasi-static approaches are often used, with no influence of the free surface effects. To conduct this study, computational fluid dynamics is used, supported by experimental results performed with a dedicated device reproducing a simplified rowing stroke in the towing tank. Comparisons show that both free surface flow and unsteadiness must be considered to capture the whole physics of the phenomenon accurately. In contrast, the viscous effects have a very limited influence.

Keywords: Rowing, oar blade, free surface flow, unsteadiness, computational fluid dynamics

Introduction

In rowing, fluid mechanics must be taken into account to investigate both the flow around the boat hull and that around the oar blades. The unsteady three-dimensional flow around oar blades, which includes violent free surface motion and overturning, appears to be the most complex modelling challenge. This physical complexity explains the relative lack of research and understanding of the hydrodynamic performance of a rowing oar blade to date.

The models of fluid forces acting on a blade that are currently used are particularly simple considering how complex the flow around the blade is. For instance, many authors still often use the very simple model suggested by Wellicome (1967) to evaluate the force on oar blades and to develop proposals for the optimization of oar setting and rowing style. This model supposes that the force is perpendicular to the blade and proportional to the square of the normal component of the instantaneous absolute velocity calculated at the centre of the blade. This quasi-static model is dimensionally consistent but the coefficient of proportionality C_n is never precisely specified.

Some work has been performed with computational fluid dynamics (CFD) by Videv and Doi (1993) to calculate this coefficient in a two-dimensional case without free surface effects, but this simplified configuration is too different from the specificity of flow around oar blades to be helpful.

Caplan and Gardner (2007a) again used a quasi-static model, but with drag and lift coefficients varying only with the angle of incidence (for a given shape of the blade). They used quarter-scale blades held static in a small water flume at a range of angles relative to the direction of the free stream to measure forces and then to deduce these dimensionless coefficients. No similarities were achieved in Reynolds and Froude numbers, implicitly considered to have negligible influence, since the results were used directly in a simulator (Caplan & Gardner, 2007b).

Research to determine the forces acting on the rowing oar blade through the stroke has been mainly experimental in nature. The physical parameters that are likely to make the deduced dimensionless coefficients vary are often ignored or not studied carefully. Moreover, they are sometimes deduced

from cases very far from real conditions. For instance, the model blade dimension and the model velocity are often different from those for real rowing, such that the Reynolds number and especially the Froude number do not match those for real rowing. In particular, the unsteadiness of the phenomenon is seldom investigated, the quasi-static approach being adopted for its relative simplicity.

Kinoshita and Kobayashi (2004) were the first to investigate unsteadiness. Although their experimental device could only generate a simplified blade motion (blade rotating around its centre in a steady flow), they highlighted that the unsteadiness of the blade motion could greatly influence the fluid force acting on the blade. They also underlined free surface effects by varying the depth of immersion of the blade.

As a consequence, the relevance of the current simplified approaches can be questioned. Are quasi-static models able to fully describe the physics of the flow? What is the influence of the free surface and the unsteadiness of the motion on forces? What about viscosity effects? How can we provide an accurate model of forces?

In the past, to answer these questions and to improve our knowledge of oar blade hydrodynamics, experimental approaches only appeared feasible, with tests in laboratories or on-water measurements. Nowadays, advances in computing power offer the possibility of relying on numerical results. The experimental investigations already available provide a useful and valuable reference database to validate CFD computations. The experimental results used here are extracted from a database on tests of oars and oar blades in a towing tank carried out at the Laboratory of Fluid Mechanics of the Ecole Centrale de Nantes (LMF UMR-CNRS 6598) by Barré (1998). Our aim is first to validate CFD computations in a configuration physically representative of a real rowing stroke. Then, free surface, unsteadiness, and viscous effects on the loads applied to the blade are studied through a numerical evaluation, before finally discussing the relevance of some physical hypotheses often stated for deducing simplified models. The software used is the ISIS-CFD solver, which has already demonstrated its capability to compute such a complex flow around an oar blade (Leroyer, Barré, Kobus, & Visonneau, 2008).

This article is organized as follows. The following section provides a description of the experimental device and presents the ins and outs of such a study. The choice of the configuration is discussed. The next section deals with the Navier-Stokes simulations; the main features of the solver are described, such as the characteristics of the different computations carried out for this specific study. The penultimate section compiles and analyses the various CFD results, by comparison with experi-

mental data. Concluding remarks and perspectives are given in the final section.

Experimental approach

General methodology of the test procedures

Instrumented boats are now commonly used to measure motions and forces on oar blades. Such tests have the advantage of working directly on a realistic configuration. However, the complexity of on-water measurements, which involve numerous and sometimes imprecisely controlled parameters, does not offer enough accuracy and repeatability to build or validate models of forces on blades. For example, it is technically difficult to measure the hydrodynamic force on a blade. Moreover, the position (or velocity) of blades is not precisely known because of oars' flexibility and variable immersion. Thus, on-water measurements have been preferred until now for comparative analysis. Another way is to reproduce the movements of blades as accurately as possible in a towing tank. This technique enables the propulsive device (the oar) to be separated from the motor (the oarsman) and from the boat, as is done for propellers. Such a system was designed at the LMF (Barré & Kobus, 1998) (see Figure 1). It is fixed on the carriage of the towing tank (dimensions: 140 m long, 5 m wide, 3 m deep) and the speed of translation is constant during the stroke. To avoid a complex mechanism, the blades remain in the water. To limit the consequences of this feature, it is possible to impose a movement (denoted by "neutral movement") calculated to minimize efforts on the blade before the catch angle of the real stroke. This technique introduces supplementary parameters such as neutral motion duration and transition phase

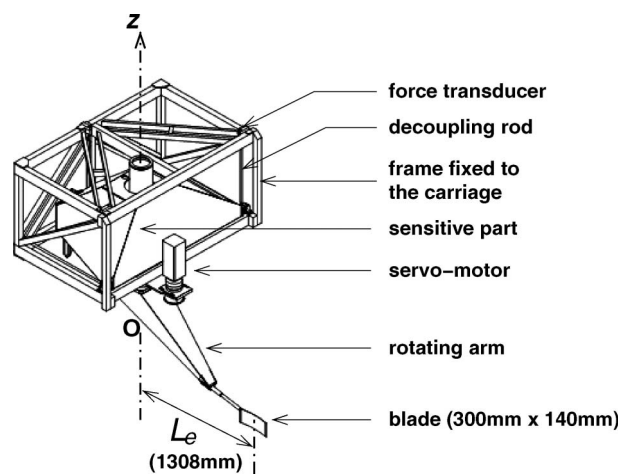


Figure 1. Diagram of the device used. Six force transducers on the frame of the dynamometer measure the forces applied on the sensitive part and transmitted by the decoupling rods.

duration (catch). To perform systematic tests, simplified movements with only two kinematic parameters can be specified. This is the case for the specific study presented here (see ‘Blade kinematics’ sub-section of this article and also Barré & Kobus, 1998).

Description of experimental device

The device is a six-component isostatic dynamometer equipped with a servo-motor and a mechanism, which reproduces a simplified motion of the oar blade in the water. It has been designed for the testing of real scull oars. However, for this study, experimental data were obtained using a model scale blade with a specific rigid arm fixed to the rotating part, which partially replaces the shaft of the oar to drastically reduce the oar flexion (see Figure 1). In this case, the blade shaft is very short and made of monolithic carbon. It is fastened to the rotary arm by a device that enables the external lever, inclination of the oar shaft, and angle of the blade with the vertical direction to be adjusted. Thus, the position of the blade in the water is precisely known.

The servo-motor and all the mobile parts are attached directly to the sensitive part of the dynamometer. Thus, any internal forces have to be taken into account. The centre of gravity of the rotating parts is located on the axis of rotation to eliminate mechanical centrifugal force. The aerodynamic forces are identified and subtracted from the measured forces. Thus, the bench test measures the three components of the hydrodynamic force on the blade directly, with an accuracy better than 0.5 N. The three components of the hydrodynamic moment are also obtained after deducting the inertial part from the measured signal. These data are stored in conjunction with the characteristics of the predefined movement. As a result, the device generates a simplified rowing stroke, but with good control of the parameters (0.3% accuracy on carriage speed and maximum deviation of 0.5% around the rate consign, repeatability within 2%). More details on the device and the experimental procedures can be found in Barré and Kobus (1998, 2009).

Choice of blade and experimental configuration for CFD comparison

With CFD, there is no limitation to take in account the real shape of the blade and the flexibility of the shaft. However, tests with flexible shafts induce additional experimental uncertainty, because the procedures and data analysis are more complex. Consequently, to make a comparison with experimental data, it is more cautious to confine the numerical study to the simpler case: a planar rectangular blade with a rigid shaft. From the

numerical point of view, this only simplifies the meshing process, since the geometry can easily and accurately be reproduced. This blade has an aspect ratio of 0.46, and its 420 cm² area S_b corresponds to a scull oar at scale 0.7.

Blade kinematics

Some notations, used in the next sections, need to be defined. For greater clarity, some of them are explained in Figure 2 and Figure 3.

The frame of reference linked to the carriage (or boat) is denoted by the orthogonal unit vectors (x_c, y_c, z) , with z oriented upward. The motion of the carriage is directed towards $-x_c$. The frame of reference linked to the blade is the orthogonal unit vectors (t, n, z) , with t the horizontal vector tangent to the blade and directed towards the rotation axis. The boat velocity (positive value) is given by $V_b = |V_b| = -V_b \cdot x_c$, whereas $V_I = V_n n + V_t t$ is the velocity of the centre of the blade. L_e means the outboard lever (>0), i.e. the distance between the rotation axis (O, z) and I the centre of blade surface.

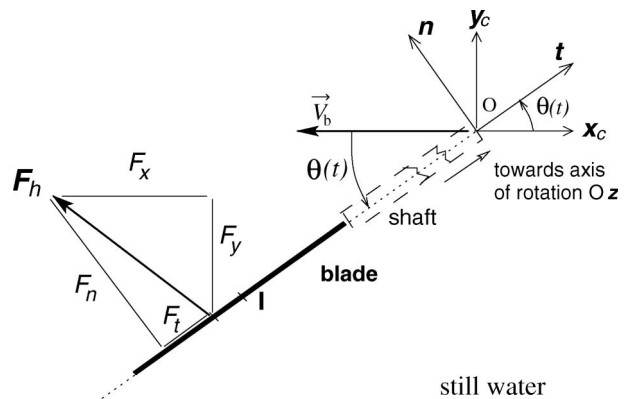


Figure 2. Definitions of axes and components of forces.

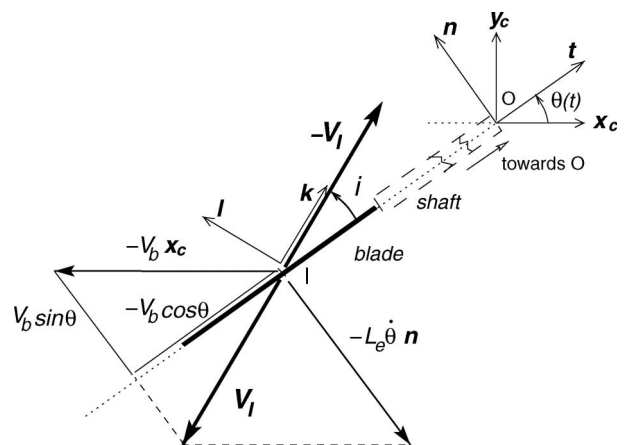


Figure 3. Definition of the pseudo-incidence at point I .

As far as angles are concerned, θ is the angle between the shaft and translational boat velocity (i.e. $(\mathbf{x}_c, \mathbf{t})$). i refers to the pseudo-incidence. This is not strictly an incidence, since its value varies along the blade, due to the rotation of the blade. It is defined by the angle of $-\mathbf{V}_I$ relative to the tangent vector \mathbf{t} (i.e. $(\mathbf{t}, -\mathbf{V}_I)$).

The horizontal hydrodynamic force \mathbf{F}_h acting on the blade has components \mathbf{F}_x and \mathbf{F}_y (respectively \mathbf{F}_t and \mathbf{F}_n) in the dynamometer (or boat) axis (respectively in the shaft axis) (see equation 1):

$$\mathbf{F}_h = F_x \mathbf{x}_c + F_y \mathbf{y}_c = F_t \mathbf{t} + F_n \mathbf{n} \quad (1)$$

\mathbf{F}_h can also be expressed in the frame (\mathbf{k}, \mathbf{l}) as drag and lift, respectively (see Figure 3): $\mathbf{F}_h = F_d \mathbf{k} + F_l \mathbf{l}$. Then, one deduces classical drag and lift coefficients:

$$C_d = \frac{F_d}{\frac{1}{2} \rho S_b V_I^2} \quad C_l = \frac{F_l}{\frac{1}{2} \rho S_b V_I^2} \quad (2)$$

To define blade movements for systematic tests, the reproduction of real measured oar movements is not suitable because these are performed with oarsmen with different rowing styles and are not linked with reliable data to the instantaneous boat speed. Furthermore, the high number of parameters that define this kind of movement makes the exploitation of test results difficult. However, even if simplified kinematics have to be used in a laboratory, it is crucial that the main physical phenomena of the real conditions are reproduced. Referring to kinematics and energetic considerations (Barré & Kobus, 2009; Leroyer et al., 2008), systematic tests were performed by imposing a significant parameter η_0 (defined by equation 3) as a constant during the whole stroke:

$$\eta_0 = V_b \sin \theta / (L_e \dot{\theta}) \quad (3)$$

As discussed by Leroyer et al. (2008), this parameter can be viewed as an advance parameter or a characteristic efficiency. The pseudo-incidence i is related to the evolution of θ with a function of η_0 . Then, we can write:

$$\begin{aligned} \tan i &= \frac{L_e \dot{\theta} - V_b \sin \theta}{V_b \cos \theta} = \tan \theta \left(\frac{L_e \dot{\theta}}{V_b \sin \theta} - 1 \right) \\ &= \tan \theta \left(\frac{1}{\eta_0} - 1 \right) \end{aligned} \quad (4)$$

The advance parameter governs the variation of the pseudo-incidence during the stroke: the higher η_0 is, the more the pseudo-incidence i varies rapidly around $\theta = 90^\circ$, but the lower is the normal component of the water velocity on the blade.

To obtain a similar flow around the blade at reduced scale and around the blade at full scale, the advance parameter and the Froude number have therefore to be respected at least in the central part of the stroke, where the unsteadiness is important. The Froude number cannot be constant for a non-steady flow and can be expressed in many ways depending on the length and velocity chosen to build it. When expressing with the chord c of the blade and the most significant flow velocity (i.e. the normal fluid velocity with respect to the blade), the Froude number is given by equation (5):

$$Fr = \frac{L_e |\dot{\theta}| (1 - \eta_0)}{\sqrt{cg}} \quad (5)$$

The choice of this reference velocity is suitable since the Froude number tends to 0 when the free surface deformation is weak, i.e. for low values of normal velocity or for kinematics close to the neutral motion ($\eta_0 \approx 1$).

The law of motion is thus imposed by the following expression:

$$\forall \theta > \theta_a, \dot{\theta} = K \sin \theta \quad (6)$$

where θ_a is small value (typically 0.01°). For angles within the range $[0, \theta_a]$, a brief linear junction law (with a constant angular velocity $K \sin \theta_a$) is applied instead of equation (6) to initiate the motion.

Finally, the kinematics of systematic tests are only defined by a couple of parameters (K, η_0) , where K represents the maximum angular velocity $\dot{\theta}_{\max}$.

Leroyer et al. (2008) have successfully compared results with experiments in the case of a very perturbed flow at low efficiency ($\eta_0 = 0.59$). In the present study, more typical parameters of a real rowing stroke were chosen to have similar flow physics compared to reality: an advance parameter η_0 equal to 0.742 and a maximum rotating rate of the real oar equal to $2.509 \text{ rad} \cdot \text{s}^{-1}$ were chosen. This leads to a boat speed of $3.478 \text{ m} \cdot \text{s}^{-1}$. The maximum Froude number at $\theta = 90^\circ$ is then 0.59. Keeping the same advance number and the Froude similitude, these parameters for the blade at scale 0.7 become $K = 3 \text{ rad} \cdot \text{s}^{-1}$ and $V_b = 2.91 \text{ m} \cdot \text{s}^{-1}$. The imposed blade trajectory under these conditions, is shown in Figure 4.

In summary, even though the test case is not based on a real rowing stroke, the flow physics of this simplified movement at reduced scale is similar to it. On the one hand, the simplified kinematics based on a constant advanced parameter enables reproduction of the typical path of the blade through the water and its unsteadiness; even if it is not a real kinematics, it is a good enough approximation for the purposes of

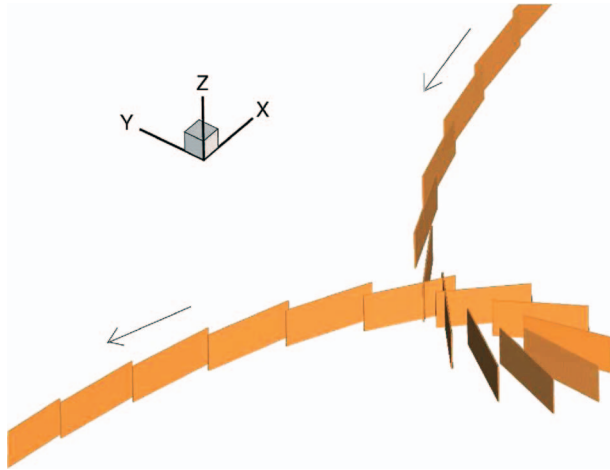


Figure 4. Prescribed motion of the blade.

this study. On the other hand, the Froude number and advance parameter are kept with respect to a full-scale stroke. The similitude is then almost complete since only the Reynolds similitude is not observed (but it is shown later in the section ‘Influence of viscous effects’ that the viscous effects are weak). As a consequence, it can reasonably be supposed that the results of the study presented here can be transposed for a rowing stroke.

Numerical approach

Flow solver

The ISIS-CFD solver, developed by the EMN (Equipe de Modélisation Numérique, i.e. the CFD Department of the Fluid Mechanics Laboratory), uses the incompressible Unsteady Reynolds-Averaged Navier-Stokes equations (URANS). The solver is based on the finite-volume method to build the spatial discretization of the transport equations. The face-based method is generalized to unstructured meshes for which non-overlapping control volumes are bounded by an arbitrary number of constitutive faces. The velocity field is obtained from the momentum conservation equations and the pressure field is extracted from the mass conservation constraint, or continuity equation, transformed into a pressure equation.

In the case of turbulent flows, additional transport equations for modelled variables are solved in a form similar to the momentum equations and they can be discretized and solved using the same principles. Here, the two-equation $k-\omega$ SST closure (Menter, 1993) was used to take into account the turbulence phenomena.

Free surface flows are computed through an interface capturing method: the flow phases are modelled through the use of a transport equation for the volume fraction (or concentration) of water c_w

in each cell ($c_w = 1$ means that the cell is completely filled with water, $c_w = 0$ means that only air is present in the considered cell). The interface between air and water is defined by the surface $c_w = 0.5$.

The effective flow physical properties (dynamic viscosity μ and density ρ) are obtained from each set of phase properties, (μ_w, μ_a) and (ρ_w, ρ_a) , for water and air respectively, with the following constitutive relations: $\mu = c_w \mu_w + (1 - c_w) \mu_a$ and $\rho = c_w \rho_w + (1 - c_w) \rho_a$.

Special attention has to be paid to preserve the sharpness of the interface when solving the transport equation of c_w . This equation is then discretized with a specific compressive scheme, including a Courant number limitation to ensure a limited diffusion of the interface (the Courant number is an adimensional parameter roughly defined by $\Delta t V = \Delta x$, where V is the velocity through the considered cell, Δx the size of the cell, and Δt is the global time step of the temporal discretization). As a result, the discretized time step has to be small enough to fulfil this CFL condition.

The solver is able to deal with the prescribed and solved motion of rigid and flexible bodies. One body with an imposed motion into an unbounded domain is involved here. This is quite a simple case, since the entire mesh can follow the body’s motion without deforming. Mesh quality is then conserved in time. Furthermore, there is no real problem of coupling due to the lack of fluid feedback on the body position. Hence, at every time step, the body is first displaced (using the prescribed law of motion), as is each node of the mesh. Then the flow is solved. Further information about the methodology is given by Leroyer (2004) and Leroyer and Visonneau (2005).

This solver has been validated in numerous validation test cases in naval hydrodynamics (Guilmineau, Queutey, Visonneau, Leroyer, & Deng, 2008) and European projects (EFFORT, Virtue). The specialized functionalities, especially those concerning the free surface and the body motions, make this solver suitable for investigating complex free surface flows.

Characteristics of simulations

Computations (denoted by dynamic cases) were carried out by imposing the prescribed law of motion of the experimental test case. Earth was chosen as the Galilean frame of reference. Hence, the translation of the carriage and the rotation of the blade are prescribed as the imposed motion of the blade (see Figure 4) and the far field velocity is then supposed to be at rest. Before launching the motion of rotation, a transient state for the motion of translation was used to raise the V_x component smoothly from zero up to the constant speed of the carriage. Next, some

other computations, denoted by static cases, were performed to be compared with unsteady configurations and so to investigate unsteadiness. The blade was then animated by the constant velocity V_I (equal to the velocity of the blade centre during the real motion at a given oar angle θ) in a fluid at rest. The procedure is then similar to the dynamic case, except that the prescribed motion is simpler, since it is a translation at a constant velocity. These static cases are finally identical to a fixed blade plunged into a uniform incident flow. Since both the geometry of the blade and the experimental prescribed motion are symmetric with respect to the angle $\theta = 90^\circ$, static cases for θ higher than $\theta = 90^\circ$ were simply deduced from results with θ lower than 90° , without further computations.

To examine the influence of the free surface, both static and dynamic tests were done with and without the presence of the free surface. For the latter, the entire domain is plunged into water and mono-fluid computations are used. Indeed, it all comes down to having a deeply immersed blade. With a Reynolds number between $3 \cdot 10^5$ and $9 \cdot 10^5$ based on the incidence velocity and the length of the blade, the flow is assumed to be turbulent in all the previous listed configurations. However, a dynamic case with free surface but under inviscid condition, denoted by *Dyn - SL - Euler*, was also performed to investigate viscous effects. Table I summarizes all the configurations tested.

All the computations (except the simulation *Dyn - SL - Euler* involving an inviscid flow) were performed using the same grid of 2,600,000 cells. This mesh was created using the software HexpressTM. Undisturbed free surface (for simulations involving this feature) is located just at the upper part of the blade, which in this case corresponds to the origin of the Z-axis. As the free surface moves along the whole surface of the blade during the motion, a

large area of grid refinement (especially behind the blade) has been added around the blade to maintain a well-defined, not too diffused, interface during the whole stroke.

A global view of the boundaries of the fluid domain (except the horizontal boundaries) is shown in Figure 5. The surface of the blade can be observed close to the middle of the fluid domain. An indication of the mesh fineness can be observed in the frame representing the surface grid on the blade. Figure 6(a) shows a horizontal section of the mesh in the middle of the blade ($Z = -0.07$ m). It illustrates the refinement area, which is more spread behind the blade where the flow is very disturbed during the stroke. Figures 6(b) and 6(c) are two magnified views of Figure 6(a) around the blade.

Boundary conditions are imposed as follows: a hydrostatic pressure is imposed (Neumann condition for both velocity and volume fraction) on the top and on the bottom of the fluid domain. On the lateral parts, velocity is imposed with its far field value, so as the volume fraction (in this case, a Neumann condition is prescribed for the pressure). Wall-function boundaries are attached to the whole surface of the blade for all turbulent flow conditions, whereas the slip condition is used for the simulation *Dyn - SL - Euler* with inviscid flow.

Here, no specific investigation has been carried out to study the grid convergence carefully. However, given the mesh size (up to 1,400,000 cells) of the previous computations described by Leroyer et al. (2008), the mesh used here (2,600,000 cells) certainly appears fine enough to discuss the influence of free surface, unsteadiness and viscous effects.

For all the simulations involving free surface effects, an adaptive time-step law was used to ensure the compressive property of the volume fraction scheme, whatever the flow velocities (Hay, Leroyer, & Visonneau, 2006).

Table I. Characteristics of the studied configurations.

Name	Viscous effects	Free surface	Dynamic case	Static case			
				θ	i	$V_I \cdot x_c$ ($m \cdot s^{-1}$)	$V_I \cdot y_c$ ($m \cdot s^{-1}$)
<i>Dyn - SL</i>	yes	yes	yes	–	–	–	–
<i>Dyn - SL - Euler</i>	no	yes	yes	–	–	–	–
<i>Dyn - NoSL</i>	yes	no	yes	–	–	–	–
<i>Stat - SL</i>	yes	yes	no	30°	11.37°	–2.52013	–0.507
				45°	19.21°	–2.05768	–0.71701
				60°	31.11°	–1.455	–0.87815
				75°	52.44°	–0.75316	–0.97945
				90°	90°	0	1.014
				105°	127.56°	0.75316	–0.97945
<i>Stat - NoSL</i>	yes	no	no	120°	148.89°	1.455	–0.87815
				135°	160.79°	2.05768	–0.71701
				150°	168.63°	2.52013	–0.507

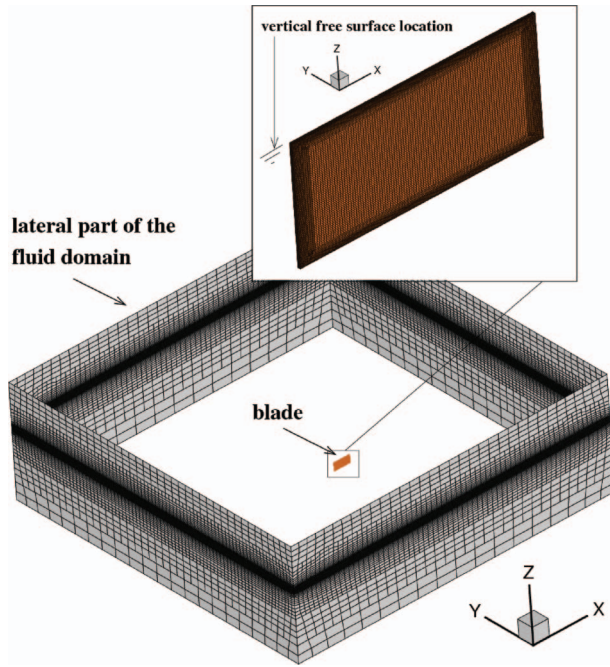


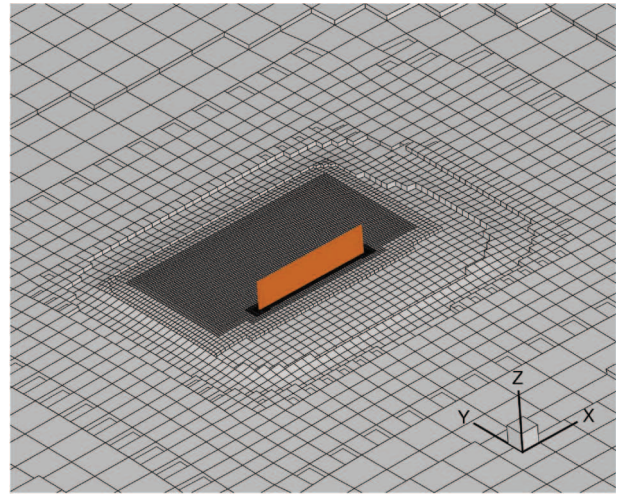
Figure 5. Global view of the boundaries of the fluid domain and surface grid of the blade.

Results and comparison

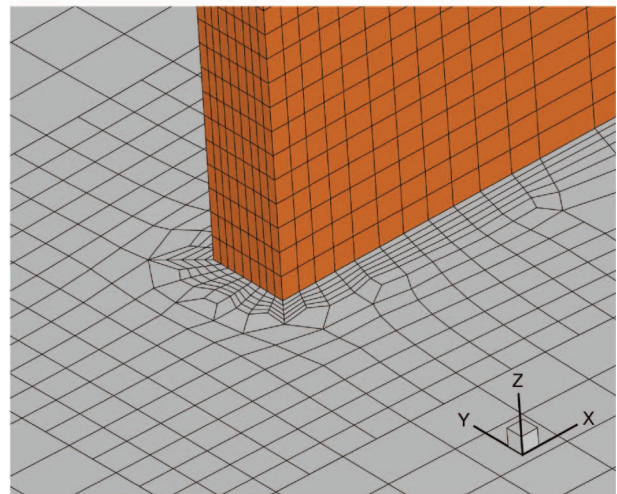
Analysis of dynamic cases

The configuration *Dyn – SL* is considered first since it represents the reference case. In fact, this simulation is the most reliable reproduction of the physics of the experimental approach, since both free surface and unsteadiness are taken into account. It is also used to validate the numerical approach by comparing the results with experimental data. At the same time, the results of the *Dyn – NoSL* will be analysed. With this case (which is the same as *Dyn – SL* but without free surface effects), we can infer the influence of free surface deformation on blade loads. This is of interest since a real stroke will be set between the *Dyn – SL* condition (blade just below the free surface) and this extreme case.

Figures 7 and 8 show the evolution of the lift and drag coefficients (see equation 2) as a function of the pseudo-incidence. Regarding the *Dyn – SL* configuration, the main physics seem to be captured, even though some differences with the experimental data can be observed. In Figure 7, a small stall is visible sooner and firmly for the experiments (at about $i = 15^\circ$). In contrast, the computation underestimates the maximum at about $i = 50^\circ$. Between 60° and 130° of incidence, the results are very similar. At the end of the propulsion, they draw apart, but maintain a similar shape. The discrepancy never exceeds 10%. For information, the uncertainties of measurement are about $\pm 3\%$. For the drag coefficient C_d , it is notable that the numerical results and



(a)



(b)

Figure 6. (a) Horizontal section of the mesh at $Z = -0.07$ m. (b) Zoom around the blade.

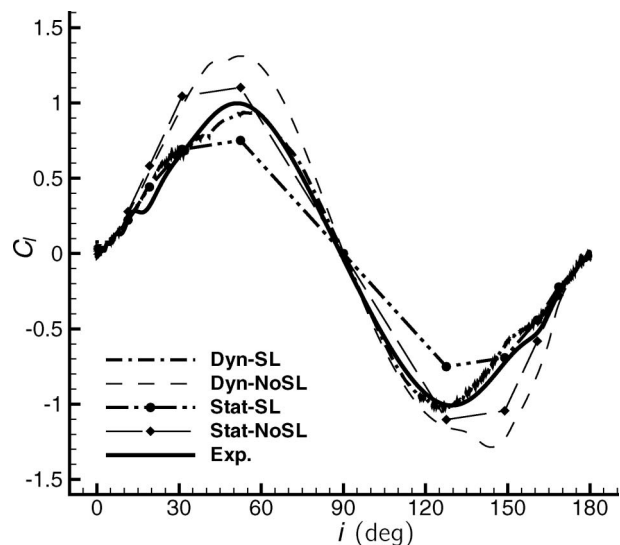


Figure 7. Lift coefficient as a function of the pseudo-incidence i .

the experimental data are close up to 70° of incidence. After that, both curves draw apart, although the global trend remains quite good. The discrepancy does not exceed 10% up to $i=90^\circ$, which is quite satisfactory (compared with the other results). However, during the dropping phase (after $i=90^\circ$), the *Dyn - SL* drag coefficient does not decrease as quickly as the experimental one. The computed drag coefficient (*Dyn - SL* configuration) appears to be more asymmetrical compared with the experimental result. In fact, we observe that the curve of *Dyn - SL* tends to catch up with the *Dyn - NoSL* curve after $i=90^\circ$. The numerical diffusion of the free surface is likely to be the cause of this anomaly. It is all the more tricky since the blade partially moves back in its own perturbed flow during this second phase of propulsion (see Figure 4). The mesh behind the blade thus seems to be too coarse to capture and convect accurately the unsteady evolution of the complex ventilated cavity until the end of the stroke (more precisely for incidence up to 90°). Due to the excessive numerical diffusion of the free surface during this phase, the perturbed flow met by the blade does not correspond to reality, but looks like something between the real ventilated cavity shape and a flow without free surface effects. The fluid forces obtained are thus between these two extreme cases. Besides, the *Dyn - NoSL* configuration around $i=90^\circ$ confirms the previous explanation: without the free surface effect (and so without numerical diffusion of this air-water interface), the behaviour is far more symmetrical. Looking more carefully at this configuration, a great similarity of the drag coefficient evolution can be observed with respect to the experimental result. Nevertheless, the values are much too high: for example, at incidence 90° , the drag coefficient C_d is around 2.7 (against 2.2

for *Dyn - SL*) whereas the experimental value is around 2.05. For the lift coefficient C_l , the behaviour at the beginning of the stroke is similar to *Dyn - SL*, and any stall is obtained at incidence 15° too. The curve is more regular compared with the *Dyn - SL* configuration between 20° and 60° of incidence. Lift is always overestimated in this configuration without free surface effects. In particular, a large overload can also be noted around $i=140^\circ$, whereas the *Dyn - SL* configuration is in far better agreement with the experimental data.

The first significant conclusion that can be drawn from these two computations (associated with the comparison with experimental data) is that the free surface has a great effect on fluid forces: it leads to a large reduction in the forces, for both lift and drag.

Figures 9 and 10 show the transverse and propulsive forces respectively as a function of the oar rotation angle θ . In fact, they are another presentation of the previous results with respect to the boat axis. This has the advantage of giving rise to the useful force for propulsion (i.e. F_x). As far as the *Dyn - SL* configuration is concerned, the transverse force F_y is well captured, but with a slight underestimation at the end of propulsion (θ between 105° and 145°), mainly due to the underestimation of C_d and C_l in the corresponding range of pseudo-incidence $130^\circ \rightarrow 165^\circ$. For the propulsive force, we observe an overestimation at the beginning and an underestimation at the end of the stroke due to the reasons presented previously. However, the general aspect of the evolution is rather satisfactory. In particular, the region where the force has higher values gives quite satisfactory results.

As a consequence, we can suppose that the solver should be able to compare the other configurations, and deduce the role played by both the physical

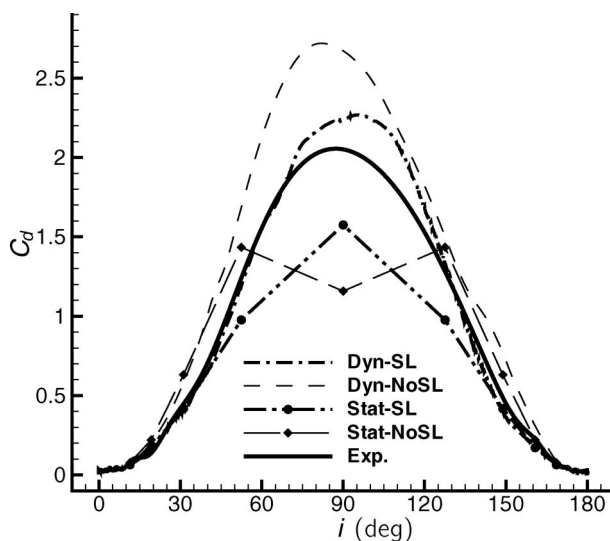


Figure 8. Drag coefficient as a function of the pseudo-incidence i .

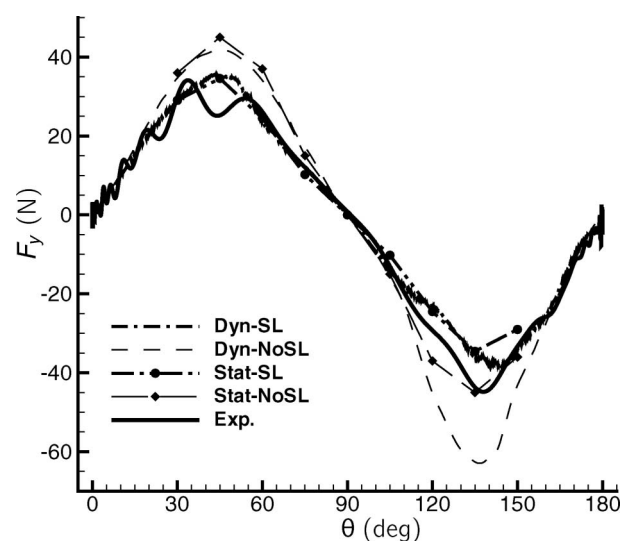


Figure 9. Transverse fluid force as a function of oar angle θ .

aspects (free surface and unsteadiness) for which no measurement is available.

For the *Dyn - NoSL* configuration, it is not surprising that the stall for F_x at around $\theta = 40^\circ$ is not captured as well. We also note that the evolution of both longitudinal and transverse forces is quite well-shaped compared with the experimental results, but with much larger values.

Analysis of quasi-static approaches

As we want to study the unsteadiness effect, the two configurations *Stat - SL* and *Stat - NoSL* are examined together since they are compared with the previous ones. The constant incident velocities correspond to the opposite of the velocity of the centre of the blade of the dynamic cases at a given oar angle. The corresponding incident velocities and incidence angles can be found in Table I. The instantaneous Reynolds and Froude numbers are thus respected for these different cases.

As expected, at the beginning of the stroke (up to about 30° of incidence), the quasi-static and dynamic approaches provide nearly identical forces (see Figures 7 and 8). However, they are perceptibly different for the same incidence at the end of the stroke because the static computations cannot take into account the flow history. Regarding lift, the quasi-static approaches underestimate significantly the values of C_L . Consequently, whereas the *Dyn - SL* results are in good agreement with experimental data, the results for the *Stat - SL* configuration are not really satisfactory, especially around 50° and 130° of incidence. However, the effect of unsteadiness is particularly crucial for the drag coefficient. Whereas up to 50° of incidence the values are still quite close to the dynamic approach and experi-

mental data, the quasi-static approach gives a value far below the experimental and dynamic results: at incidence 90° , we obtain 1.15 for the *Stat - NoSL* configuration (coherent with experimental values that can be found in the literature, see, for example, Hoerner, 1965) and 1.55 for the *Stat - SL* configuration. They are very far from the experimental value ($C_d = 2.05$). In Figure 8, an inversion of curvature for the quasi-static case without free surface *Stat - NoSL* is even visible.

These observations are confirmed in Figures 9 and 10. For the transverse force F_y , both approaches (static and dynamic) give similar results in the first part of the stroke up to $\theta = 90^\circ$. In the second part, the differences remain quite limited for the computation including free surface effects (*Stat - SL* vs. *Dyn - SL*), whereas the computation without free surface *Stat - NoSL* leads to a large underestimation of F_y for the quasi-static approach compared with the dynamic one. For the propulsive force, the quasi-static approach gives acceptable results up to $\theta = 60^\circ$, but leads to a larger decrease of the force between 60° and 120° (i.e. in the working region of the blades). Here again, the decrease is larger in the quasi-static case without free surface (*Stat - NoSL*).

Analysis of polar curves and discussion

Finally, to compile the comparisons between the different approaches, the reader should refer to Figure 11. This graph shows clearly that the quasi-static approach is ineffective, especially for the drag coefficient. The unsteadiness has a great influence on keeping higher values around $\theta = 90^\circ$, whether the free surface is considered or not. This study also shows that the immersion of the blade (i.e. the presence of the free surface) has a significant

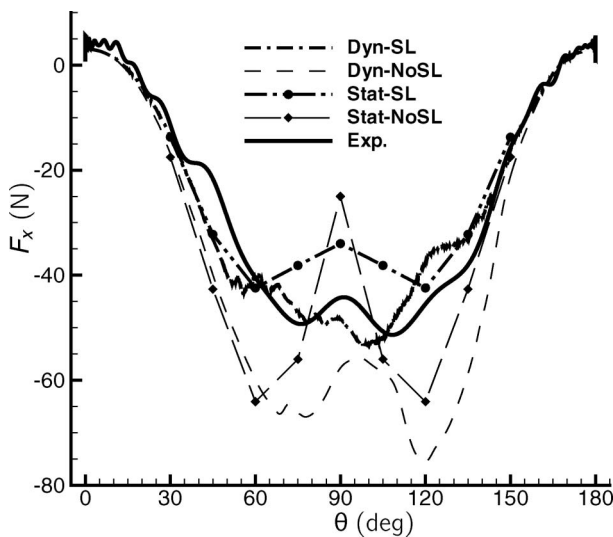


Figure 10. Propulsive fluid force as a function of oar angle θ .

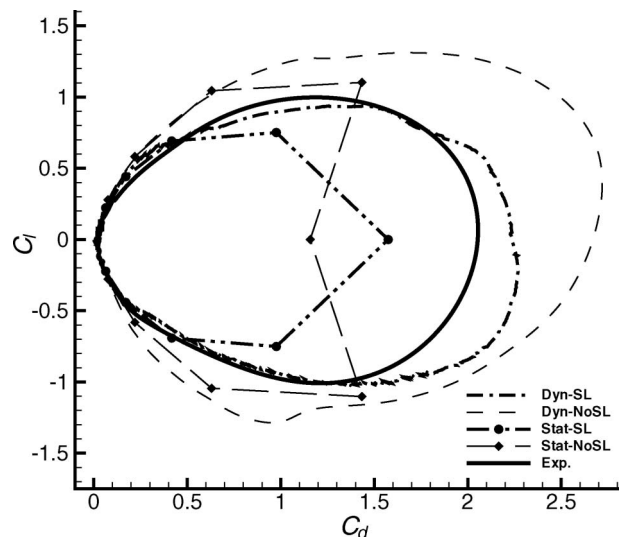


Figure 11. Polar curve.

Downloaded By: [Kobus, Jean-Michel] At: 16:24 13 October 2010

influence on both lift and drag coefficients. As a consequence, this factor should be taken into account to estimate accurately the load on the blades during a real stroke.

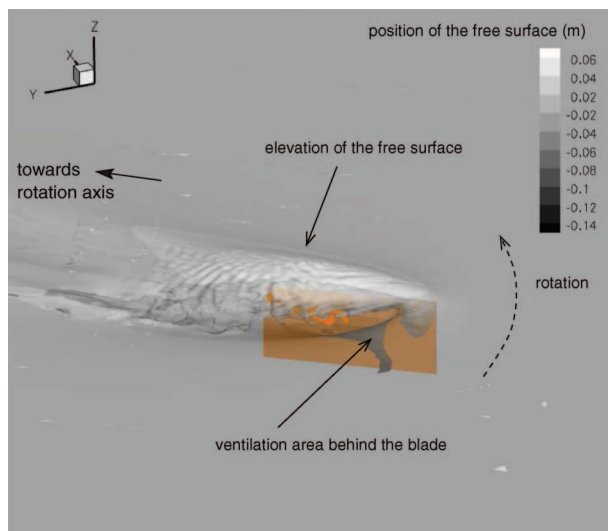
Figure 11 also underlines that only the dynamic configuration with free surface *Dyn - SL* leads to acceptable results compared with the experimental data even if, as previously noted, it suffers from too much numerical diffusion of the free surface.

In the literature, few results dealing with these two crucial physical features (unsteadiness and free surface effects) are found. Only Kinoshita and colleagues (Kinoshita & Kobayashi, 2004; Kinoshita, Miyashita, Kobayashi, & Hino, 2006) present a set of measurements and computations about this issue. It is difficult to compare their values (for example, the drag coefficient), because their configuration is slightly

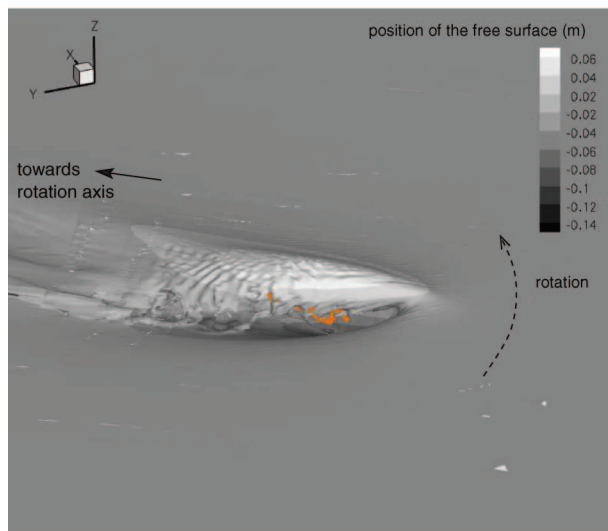
different: the blade is also a planar one, but the aspect ratio is different (0.46 here against 0.57 for Kinoshita and Kobayashi, 2004), as are the kinematics, since the blade turns around this centre in a uniform flow. However, we remark that the observed trends and conclusions are similar: the drag force is much lower around $\theta = 90^\circ$ in the dynamic tests compared with the quasi-static case, and the immersion increases significantly the maximum value of the drag.

Features of the flow

As the *Dyn - SL* configuration is the only valid approach to include all the physics of the flow around a rowing blade, the computed flow is now examined. Simulation exhibits a very complex evolution of the free surface. Figures 12 and 13 represent the free

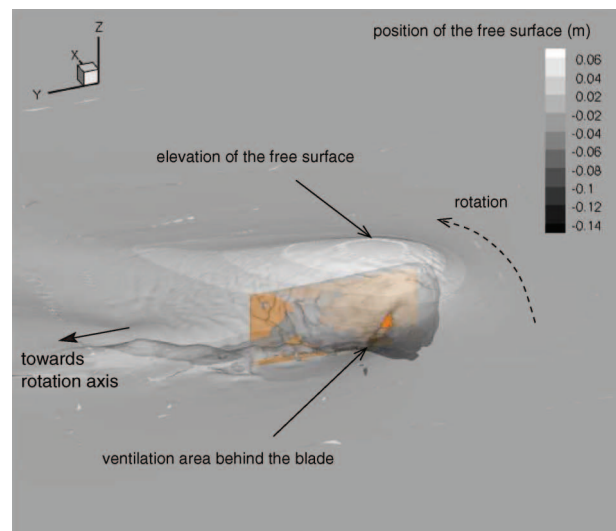


(a)

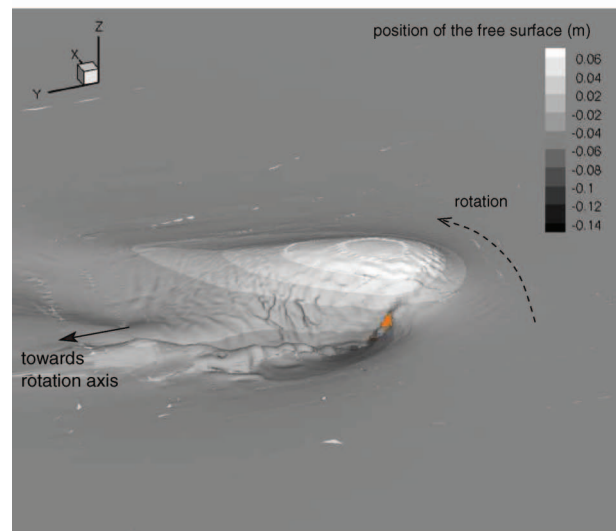


(b)

Figure 12. Free surface for $\theta = 60^\circ$. (a) With transparency; (b) without transparency.



(a)



(b)

Figure 13. Free surface for $\theta = 90^\circ$. (a) With transparency; (b) without transparency.

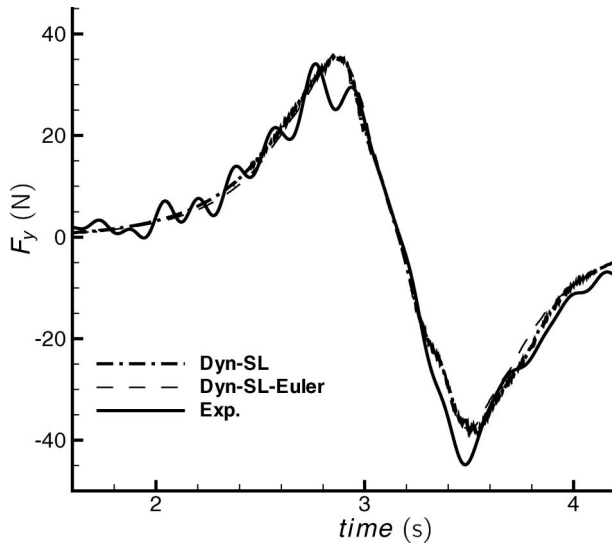


Figure 14. Transverse force as a function of time.

surface for $\theta = 60^\circ$ and $\theta = 90^\circ$ respectively. An elevation of the free surface just behind the inflow side of the blade can be observed. As a result, a flow with a conical shape can be noted passing above the upper part of the blade (see Figure 12). Simultaneously, the low pressure generated on the other side of the blade leads to the formation of a bowl-shaped cavity. During the stroke, the free surface moves down to the bottom of the blade, generating a large ventilated cavity. In view of this complex free surface evolution, it is not surprising that the numerical diffusion is too large.

Influence of viscous effects

Using the finer mesh (1,400,000 cells) designed by Leroyer et al. (2008), a final computation was performed with an inviscid hypothesis (denoted by *Dyn - SL - Euler*) to determine whether viscosity (and turbulence induced) has no critical physical features for application of that kind. Indeed, Figures 14 and 15 show a very limited effect between the inviscid and viscous simulation, particularly concerning F_y . The differences for the propulsive force F_x are slightly more sensitive: in the part where the blade is nearly aligned with the flow velocity (at the beginning and at the end of the motion), the viscous turbulent model is obviously in better agreement with experiments since viscous drag is the paramount effect in this configuration. During the working phase of the rowing stroke, turbulence seems to have an influence only during the dynamic “stall stages” (around $t = 3$ s and $t = 3.4$ s).

Due to the Boussinesq approximation of the $k-\omega$ SST closure used here, the turbulent model simply increases the molecular viscosity by a local “turbulent” viscosity deduced from the resolution of

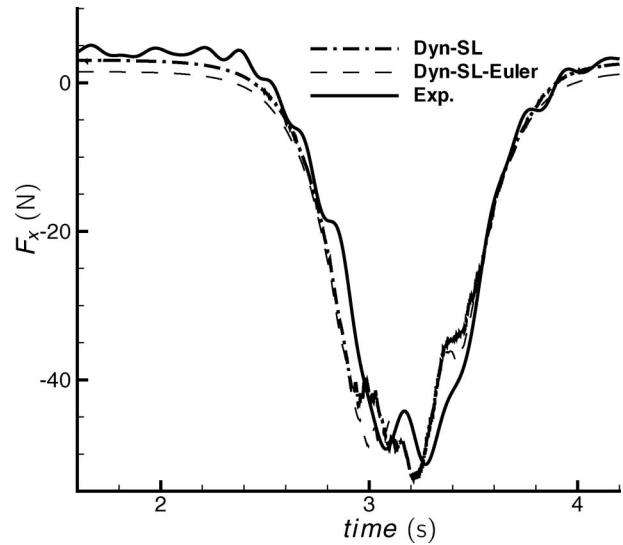


Figure 15. Propulsive force as a function of time.

these two extra variables k and ω . Compared with a laminar flow, the effective viscosity is then higher and non-uniform. Since the results assuming a turbulent flow and an inviscid flow are very similar, the weak role played by viscous effects is here clearly identified.

Conclusions

The aim of this study was to examine the influence of free surface and unsteadiness effects on the hydrodynamic forces acting on the blade during a rowing stroke. With this aim in mind, four kinds of computations were carried out: a reference configuration taking into account both effects, a configuration where the blade is moving with the same motion but without free surface effects, and two quasi-static configurations (with and without free surface). These numerical results were then compared with each other and with experimental data obtained from a dedicated device reproducing a simplified rowing stroke. A planar blade with a rigid shaft at scale 0.7 was chosen for the sake of simplicity and to avoid further physical complexities, such as the flexibility of the oar. In spite of these simplifications the flow obtained around the blade is representative of the greater part of the physical phenomenon that occurs during a real oar stroke. This is a major point since the objective is to validate a numerical modelling of such a flow.

The analysis of the results clearly demonstrates that both free surface and unsteadiness effects are crucial features. Without one of these physical aspects, computations fail to reproduce the real behaviour of the blade loads, especially for the propulsive part along the boat axis. In contrast, the configuration taking into account both free surface

and unsteadiness effects is the only one to agree reasonably well with experimental data. The remaining differences may be explained by too much numerical diffusion.

The real-life situation of a rowing blade involves unsteady free surface flow and time-dependent translation and rotation motions. It would appear that static models cannot model blade forces correctly in the middle of the stroke: they underestimate the propulsive component between 70° and 110° oar angle, where the major part of the propulsion occurs. In addition to the unsteadiness, these results highlight major free surface effects (in relation to the immersion of the blade). As a consequence, these two aspects should be part of a reliable simplified model of forces. As the phenomenon is complex, it is not surprising that more complex models need to be developed. Lastly, it has been shown that, contrary to the two previous physical aspects, viscous effects are negligible, as previously reported by Leroyer et al. (2008): it seems that the Reynolds number is not a significant parameter of this kind of flow. The numerical simulations presented here show the capacity of modern viscous solvers to deal with such a complex flow. Even if grid convergence is not totally obtained, comparisons with experimental data are very encouraging and offer hope concerning the capacity of the numerical method to simulate such a flow pattern accurately. The fact that the elevation and shape of the free surface change extensively during the stroke makes the task more difficult. More advanced numerical methods have to be achieved to perform accurate simulations within a reasonable computational time. In the future, CFD may thus provide extra useful information, especially at full scale and for complex situations, where physical experimentation reaches limits. Indeed, the study of complex movement with variable immersion (with catch and finish) and with variable speed of translation should be taken into account far more easily than can be done experimentally. It will then be a useful tool to calibrate a reliable and accurate model of forces. A better understanding of the physics of the flow around an oar blade will also be gained through the comparison of realistic configurations and CFD computations.

Acknowledgements

This work was granted access to the HPC resources of IDRIS under the allocation 2009-000129 made by GENCI (Grand Equipement National de Calcul Intensif).

References

- Barré, S. (1998). *Etude expérimentale des systèmes de propulsion instationnaire, application aux palettes d'avion*. Unpublished doctoral dissertation, University of Nantes/Ecole Centrale de Nantes.
- Barré, S., & Kobus, J. (1998). New facilities for measurement and modelling of hydrodynamic loads on oar blades. In S. Haake (Ed.), *The engineering of sport* (pp. 251–260). Oxford: Blackwell Science.
- Barré, S., & Kobus, J. (2009). Comparison between common models of forces on oar blades and forces measured by towing tank tests. *Journal of Sports Engineering and Technology*, 224, 37–50.
- Caplan, N., & Gardner, T. (2007a). A fluid dynamic investigation of the Big Blade and Macon oar blade design in rowing propulsion. *Journal of Sports Sciences*, 25, 643–650.
- Caplan, N., & Gardner, T. (2007b). A mathematical model of the oar blade–water interaction in rowing. *Journal of Sports Sciences*, 25, 1025–1034.
- Guilmineau, E., Queutey, P., Visonneau, M., Leroyer, A., & Deng, G. (2008). RANS simulation of a US Navy frigate with PMM motions. Presentation to the *Workshop on Verification and Validation of Ship Maneuvring Simulation Methods, SIMMAN 2008*, Copenhagen, April.
- Hay, A., Leroyer, A., & Visonneau, M. (2006). H-adaptive Navier-Stokes simulations of free-surface flows around moving bodies. *Journal of Marine Science and Technology*, 11, 1–18.
- Hoerner, S. F. (1965). *Fluid dynamic drag*. Bakersfield, CA: Hoerner Fluid Dynamics.
- Kinoshita, T., & Kobayashi, H. (2004). Improving rower motion and rowing equipment by using rowing velocity prediction program with estimating hydrodynamic load acting on an oar blade. *International Journal of Small Craft Technology*, 146, 16–26.
- Kinoshita, T., Miyashita, M., Kobayashi, H., & Hino, T. (2006). Rowing velocity prediction program with estimating hydrodynamic load acting on an oar blade. In *Third International Symposium on Aero Aqua Bio-mechanisms*. ISAB-MEC 2006.
- Leroyer, A. (2004). *Fluid/motion interaction for solid and flexible bodies by resolution of the Navier-Stokes equations: Contribution to the numerical modelling of cavitating flows*. Unpublished doctoral dissertation, University of Nantes/Ecole Centrale de Nantes. Retrieved from ftp://ftp.ec-nantes.fr/pub/DMN/Thesis/these_leroyer.pdf (in French).
- Leroyer, A., Barré, S., Kobus, J. M., & Visonneau, M. (2008). Experimental and numerical investigations of the flow around an oar blade. *Journal of Marine Science and Technology*, 13, 1–15.
- Leroyer, A., & Visonneau, M. (2005). Numerical methods for RANSE simulations of a self-propelled fish-like body. *Journal of Fluids and Structures*, 20, 975–991.
- Menter, F. (1993). Zonal two-equation $k - \omega$ turbulence models for aerodynamic flows. In *24th AIAA Fluid Dynamic Conference*, Orlando, FL, July.
- Videv, T., & Doi, Y. (1993). Unsteady viscous flow simulation around the blade of rowing boat. *Journal of the Society of Naval Architects of Japan*, 173, 97–108.
- Wellcome, J. (1967). Some hydrodynamic aspects of rowing. In J. G. P. Williams & A. C. Scott (Eds.), *Rowing: A scientific approach* (pp. 22–63). London: Kaye & Ward.